Electronic Supplementary Material (ESI) for Soft Matter.

Supplementary Material

Effects of lipid composition on membrane permeation

Michail Palaiokostas,[†] Wei Ding,[†] Ganesh Shahane,[†] and Mario Orsi[*,‡]

[†]*School of Engineering and Materials Science, Queen Mary University of London, London, UK*

[‡] *Department of Applied Sciences, University of the West of England, Bristol, UK*

E-mail: mario.orsi@uwe.ac.uk

Properties of examined molecules

Table S1: Physical properties of the permeating molecules

Molecule		MW [g/mol]	HB Dn	HB Ac	TPSA [Å^2]	HA	Exp $\mathbf{LogP_{o/w}}$	CAx $\mathbf{LogP_{o/w}}$
Ammonia	NH_3	17.03	1	1	13.6	1		-0.98
Water	H_2O	18.02	1	1	25.3	1	-1.38†	-0.65
Fluoromethane	CH_3F	34.03	0	1	0	2	0.51*	0.37
Carbon dioxide	CO_2	44.01	0	2	34.1	3	0.83†	-0.28
Propane	C_3H_8	44.10	0	0	0	3	2.36†	1.8
Ethanol	C_2H_6O	46.07	1	1	20.2	3	-0.30*	-0.16
Urea	CH_4N_2O	60.06	2	1	69.1	4	-2.11†	-1.36
Isopropanol	C_3H_8O	60.10	1	1	20.2	4	0.05*	0.25
Glycine	$C_2H_5NO_2$	75.07	2	3	63.3	5	-3.21†	-3.41
Phenol	C_6H_6O	94.11	1	1	20.2	7	1.50*	1.67
Benzoic Acid	$C_7H_6O_2$	122.12	1	2	37.3	9	1.87*	1.63
Coumarin	$C_9H_6O_2$	146.15	0	1	26.3	11	1.39†	1.78
Paracetamol	$C_8H_9NO_2$	151.17	2	2	49.3	11		0.91

MW: Molecular weight
HB Dn: Number of hydrogen bond donors
HB Ac: Number of hydrogen bond acceptors
TPSA: Topological polar surface area
HA: Number of heavy atoms (non-hydrogen)
Exp $\mathbf{LogP_{o/w}}$: Experimental logarithm of octanol/water partition coefficients
CAx $\mathbf{LogP_{o/w}}$: Computed octanol/water partition coefficient with the ChemAxon logP[1] QSAR online tool "Chemicalize" (`http://chemicalize.com`)

$*$: Reference[2]
† : Reference[3]

Convergence of simulations

Establishing a convergence evaluation technique

According to the inhomogeneous solubility diffusion model, the exponential of the free-energy difference is the dominant factor in the computation of the permeation coefficient and as such, it was chosen as the key property to examine simulation convergence. However, the restrain force and the derived potential of mean force are dynamic properties that fluctuate during the simulation. In fact, statistically, due to the nature of MD simulations, these properties can never be considered absolutely converged due to the fact that ergodicity is an assumption and the complete exploration of phase space is impractical or impossible.[4]

In this study we devised a new method to measure relative convergence. The restrain-force timeseries was separated in 10 consecutive cumulative parts starting from the beginning of the timeseries and then each consecutive part was added in the timeseries used to produce the free-energy profile. Figure S1 visualises how this approach works. With this method both quantitative and qualitative convergence was revealed clearly after the first 3 cumulative sets, damping sampling noise.

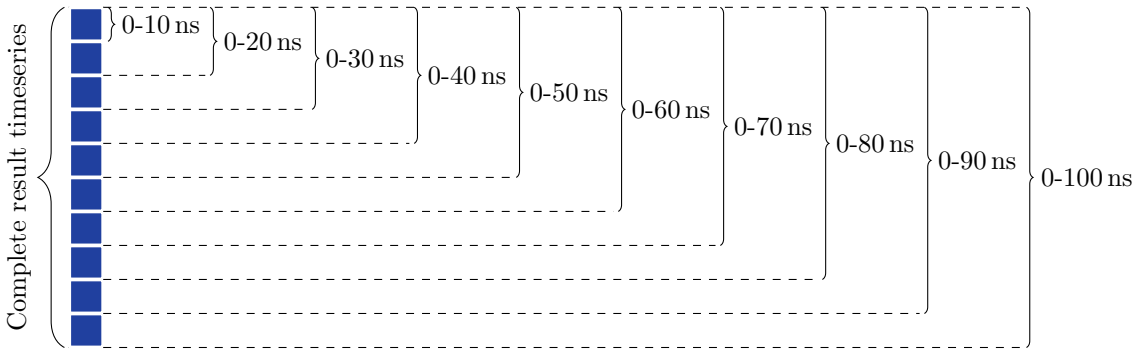

Figure S1: Schematic of the convergence study technique with cumulative sets of the time-series.

Similar methodologies have been used in previous studies. Bemporad et al.[5–8] have examined the behaviour of force timeseries to ensure its convergence to a particular value. Neale et al.[9] have used the block averaging[10] method to identify the equilibration time based on the

initial systematic errors. On the same article, they propose the definition of a key observable, such as the binding free-energy, and the estimation of convergence based on its behaviour as a function of simulation time. Nitschke et al.[11] defined as the key observable in their study of ammonia and ibuprofen, the PMF barrier and minimum respectively. Paloncỳovà et al.[12] used a contour plot showcasing the time evolution of the energy minima and barriers with their respective positions. Carpenter et al.[13] used a variation of the moving-average method to examine the convergence of free-energy profiles. Finally, Lee et al.[14] observed that simulation over the whole range of the bilayer thickness instead of half, even for shorter time, generally improved convergence speed. They also recommended a 50 to 100 ns equilibration for each window. It is clear from the aforementioned studies that there is no established methodology in the literature regarding the convergence of permeation studies. Therefore, the results presented in this paper can provide researchers with an extra insight on this crucial parameter.

Convergence study

Figures S2 and S3 show the evolution of the free-energy profile of the DOPC and DOPC:DOPE (1:3) membranes and all permeants, for the z-restraint method. Generally profiles stabilise between the 0-30 ns and 0-40 ns blocks. Initial blocks fluctuate more because the permeant-membrane complex relaxes to accommodate the new restraint behaviour of the permeant. Also, they are relatively more noisy than the latter blocks because the number of sampled points is smaller. Nevertheless, even in the worst case of urea and the DOPC membrane, the maximum ΔG fluctuation between the initial block of 0-10 ns and the stable block of 0-40 ns is $\approx$3 kcal mol^{-1} and localised only on the bilayer centre. Qualitatively, profile fluctuations are more prominent in fluoromethane or carbon dioxide but this is due to the small scale of the y-axis which amplifies the differences. Based on the above, the first 30 ns of the production trajectories and outputs were discarded as further equilibration.

For most permeants the convergence was 10 to 15 ns faster through the pure DOPC than

through the mixture and the difference was particularly evident for the largest permeant, phenol, benzoic acid, coumarin and paracetamol. However, the same or slower convergence for the permeation through DOPC was observed for fluoromethane, carbon dioxide and isopropanol. Slower convergence for bilayers of mixed composition has also been observed in a study of Hong et al.[15] where they examined the total time for complete mixing of various lipids in symmetrical bilayers. They saw that the radial pair distribution function of PE:PG and PC:cholesterol membranes was slower to converge than that of pure POPC.

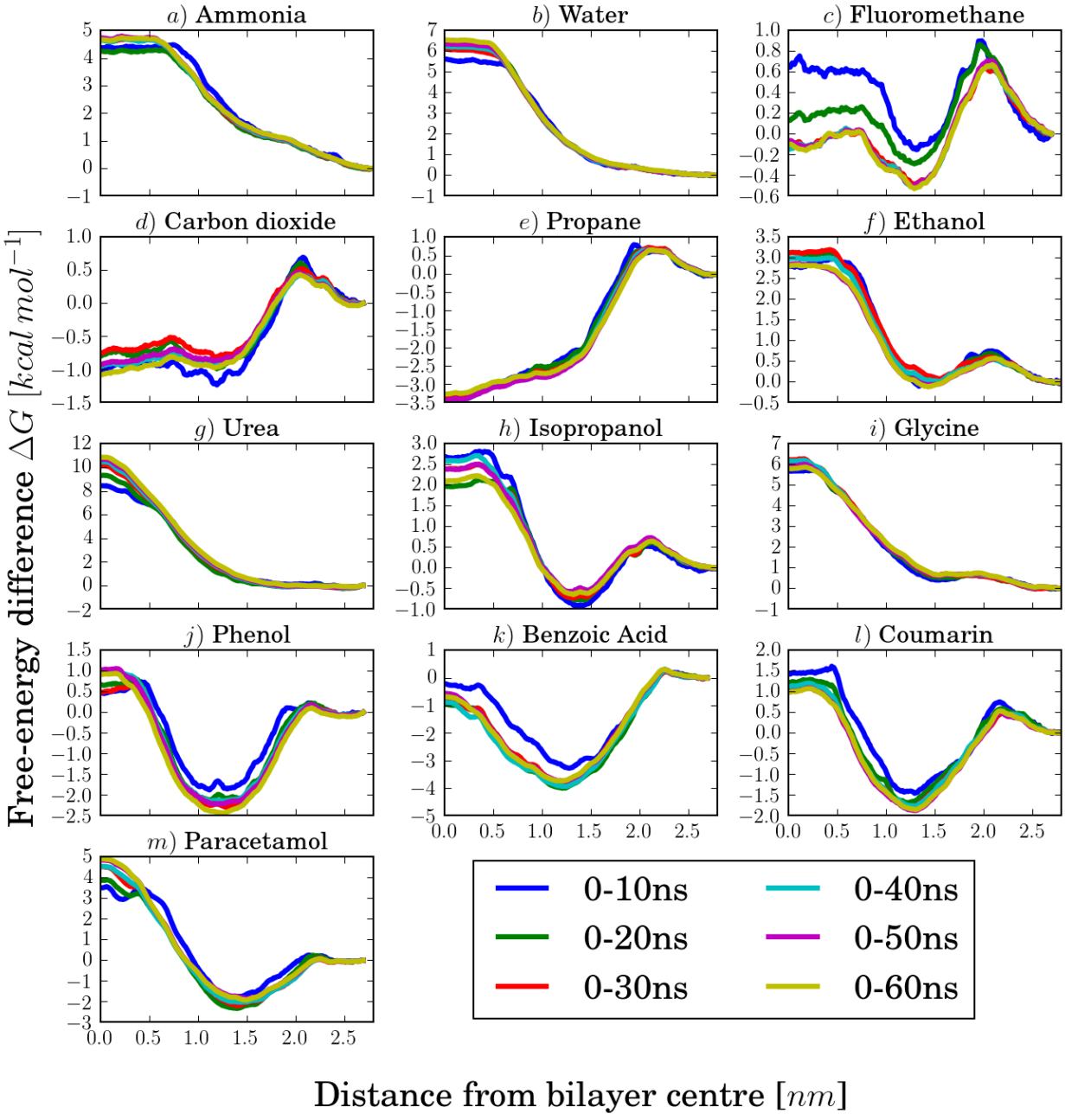

Figure S2: Convergence of ΔG for all permeants and the DOPC membrane

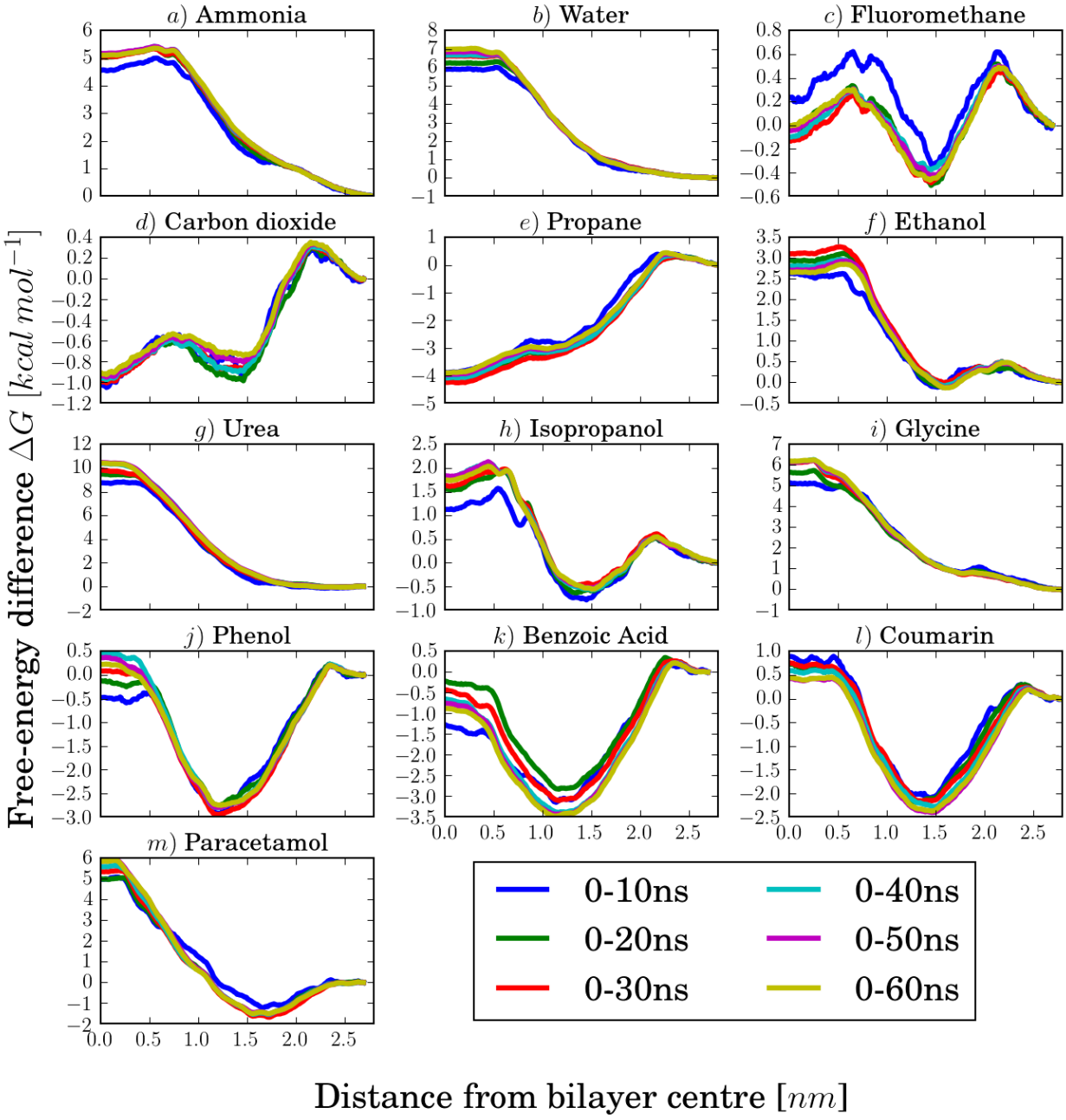

Figure S3: Convergence of ΔG for all permeants and the DOPC:DOPE(1:3) membrane

Local diffusion coefficients analysis

Hummer method analysis

The method proposed by Hummer requires the calculation of the integrated autocorrelation function τ of the z-axis distance between the permeant and the membrane's centre of mass, for each 10 ns part of the z-position timeseries (7 in total from 30 ns to 100 ns). While the computation of the autocorrelation function is trivial due to pre-existing numerical libraries, the calculation of the integral poses a challenge. A practice that has been used previously [5,13] involves the fitting of a double exponential function to the autocorrelation of the z-axis distance. Unfortunately, when it was attempted to fit a double exponential function to different 10 ns autocorrelation values of the z-axis distance, the fitting failed partially or completely (figures S4a, S4b and S4c). Reduction of the autocorrelation datasets from 10 000 to 1000 did not improve the overall poor performance of the fitting (figures S4d, S4e and S4f).

O'Neill et al. [16] have examined an alternative technique for the calculation of the autocorrelation function integral. Instead of fitting, they used 4 different cut-offs in order to decide the integration domain (the length of the autocorrelation dataset), which was then integrated numerically with the trapezoidal rule. In the first cut-off, the entire autocorrelation dataset was considered for the integral, the second included the values until the global minimum of the negative values, the third included the values until the first time that autocorrelation became zero and finally the fourth took into account all values until when autocorrelation became smaller than 1/e. Table S2 presents the results for the DOPC-water system, for 4 different distances from the bilayer core and for the 4 different techniques.

When considering the whole extent of the autocorrelation (9999 points for a 10 ns timeseries) the calculated diffusion coefficients were nonphysical, due to the long oscillatory behaviour of the decay tail. The fourth method overestimated diffusion coefficients especially in the hydrophobic region of the bilayer, that for water are usually much smaller [7,17] than

$1\,\mathrm{cm\,s^{-2}}$. Also, for fast decaying autocorrelations, the 1/e criterion was very high and was a potential source of error. Finally, the other 2 methods produced similar, physically plausible values, however, in cases where the autocorrelation never becomes negative or it has multiple minima, the ACF = $\mathrm{ACF_{min}}$ criterion becomes problematic.

Table S2: Evaluation of the integral domain for the Hummer method based on the work of O'Neill et al.[16]

	D [x10^{-5} cm^2/s]			
Integration domain	z=0.1 nm	z=1 nm	z=2 nm	2.8 nm
x = xmax	237305	504341	-198962	151866
x at ACF = $\mathrm{ACF_{min}}$	2.06	0.15	0.8	4.26
x at ACF = 0	1.48	0.13	0.53	3.38
x at ACF = 1/e	3.98	1.63	2.31	4.59

In order to examine whether the fitting performance would be better for a smaller autocorrelation dataset, the x at ACF = 0 criterion was used in conjunction with a double exponential fitting. Figure S5 shows that with a smaller number of points, the fitting behaviour improved, however, the computed diffusion coefficients were orders of magnitude lower than expected.

In conclusion, regarding the Hummer method for the calculation of diffusion coefficients, the integral domain for x at ACF = 0, with no fitting, is preferred for its robustness and general applicability independent of the ACF behaviour.

DOPC diffusion profiles oscillations

It has been noticed from previous studies[6,7,13,18–20] that local diffusion profiles are more noisy than the respective free-energy difference profiles. In this study, this behaviour is predominant in the DOPC rather than the PC:PE profiles. Especially for water, fluoromethane, propane, urea, isopropanol and benzoic acid there is an protruding peak at 2.3 nm away from bilayer centre, which has not been observed in past studies. Figure S6 shows the restrained z-position timeseries that the simulation for the DOPC-water system produced for two dif-

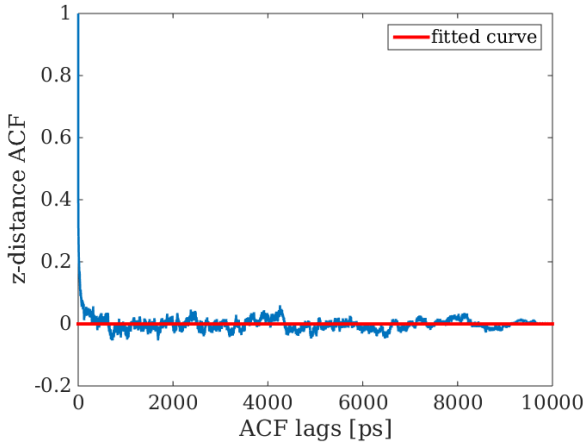

(a) 10 ns. Complete failure.

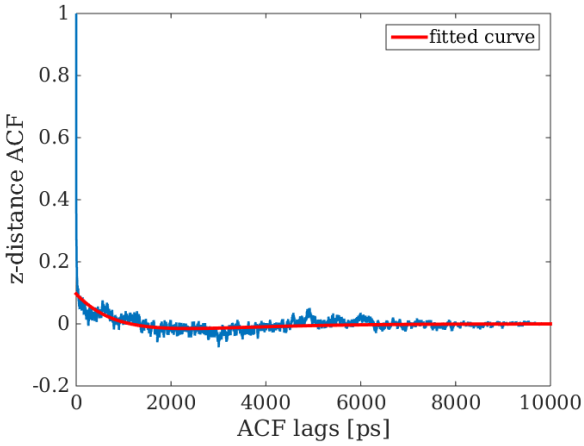

(b) 10 ns. Missed initial part.

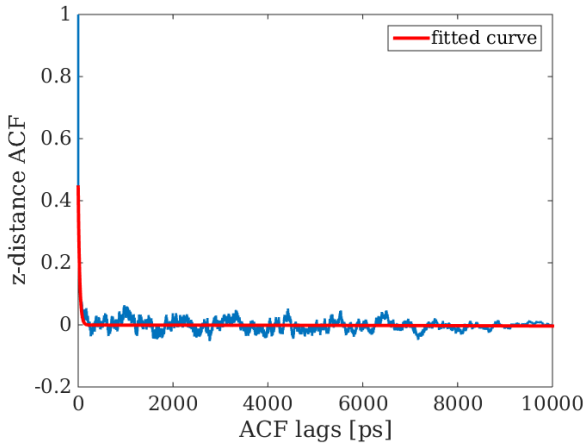

(c) 10 ns. Partial fit through initial part.

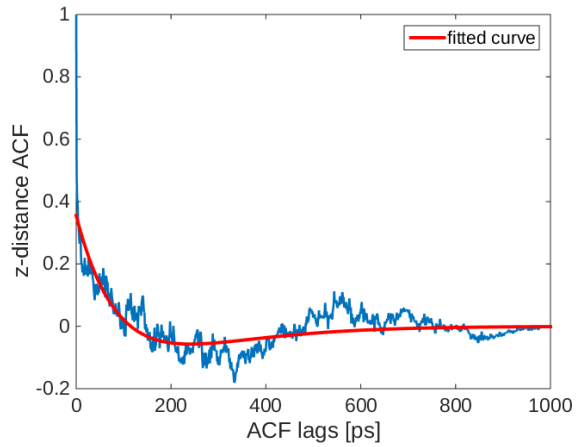

(d) 1 ns. Partial fit through initial part.

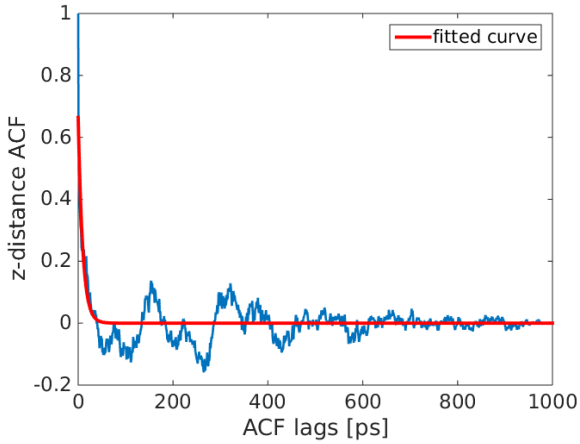

(e) 1 ns. Negative-positive fluctuation.

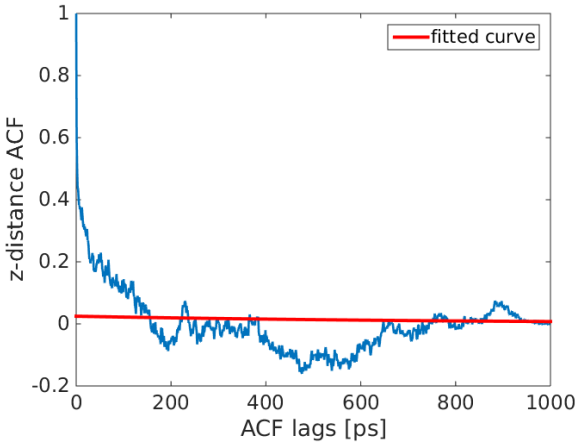

(f) 1 ns. Complete failure.

Figure S4: Common problems encountered when attempting to fit a double exponential function to a 10 ns or a 1 ns part of the clean z-distance autocorrelation. The system is the DOPC-water and the autocorrelation is between 90 ns to 100 ns.

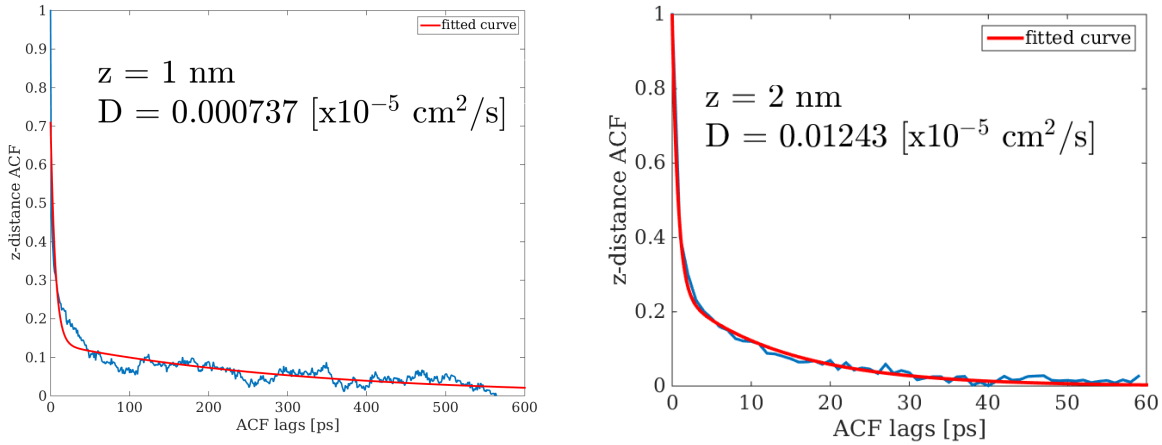

(a) 1 nm. Lost initial part.

(b) 2 nm. Good fit. Wrong D.

Figure S5: Fitting of a double exponential function to a filtered z-distance autocorrelation. The system is the DOPC-water and the acf is from 90 ns to 100 ns

ferent positions, 1.8 nm and 2.3 nm. In the 2.3 nm timeseries (orange line) there is a highly oscillatory behaviour between 55 ns and 75 ns where the water permeant moved further than the typical ±0.15 nm from the average position. Figure S7 shows 4 trajectory (sampling every 10 ps) snapshots from this time range. Apart from random crosses through the periodic boundary conditions (figure S7b), no obvious facilitators or bilayer structural irregularities were observed to explain this behaviour.

To examine whether manual removal of extreme outliers of the timeseries would improve the diffusion results, a filter was applied to the data to discard all z-restrain position that were deviating more than ±0.15 nm from the average position. Figure S6 shows the effect of the filter on the 2.3 nm timeseries and table S3 presents the diffusion coefficients and the percentage of timeseries that were outliers for three representative timeseries. Overall, for the cases that the rejection percentage was low, the effect on diffusion was marginal. In the case of z=2.3 nm, diffusion was reduced by ≈ 18%, however, even with the filter applied the diffusion value was still higher than in the neighbouring points. Considering that a filter can introduce other biases or artifacts on the results, it was decided not to implement filtering on the calculation of diffusion coefficients.

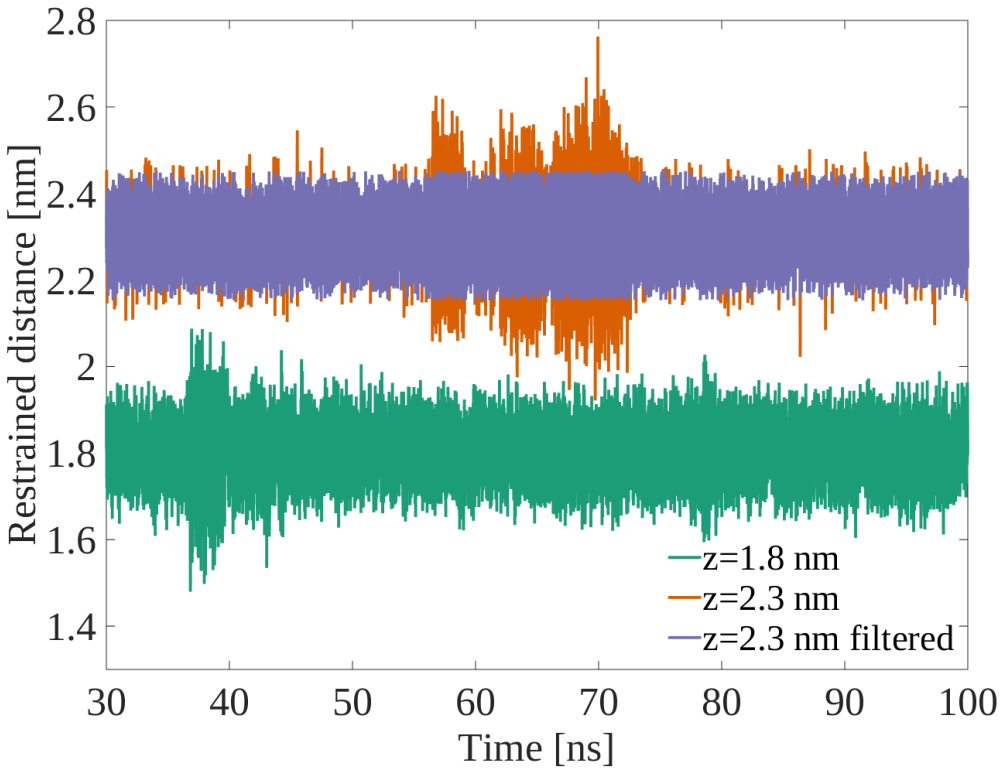

Figure S6: The restrained z-position timeseries for the z=1.8 nm and z=2.3 nm positions and the DOPC-water system. Also, the effect of applying an 'exclude-outliers' filter in the z=2.3 nm timeseries.

Table S3: Effect of an 'exclude-outliers' filter in the diffusion coefficients. The outliers value shows the percentage of data that were discarded from the original timeseries.

	D [x10^{-5} **cm**^{2}/**s**]		
z [nm]	*Original*	*Filtered*	*Outliers*
1.8	0.4	0.4	0.6%
2.2	1.5	1.5	0.7%
2.3	2.7	2.2	1.7%
2.4	1.5	1.5	0.3%

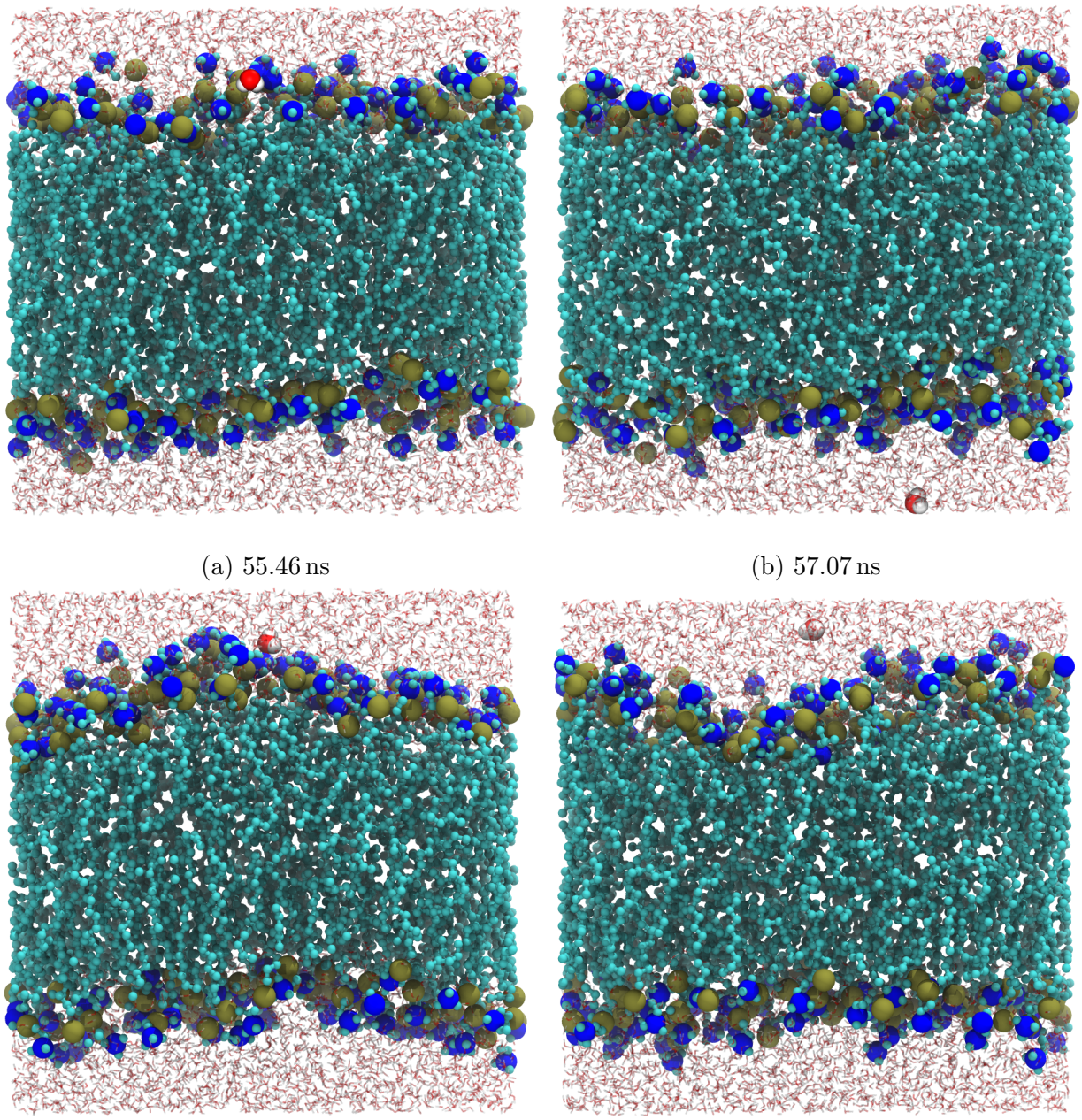

(a) 55.46 ns

(b) 57.07 ns

(c) 62.49 ns

(d) 70.00 ns

Figure S7: Trajectory snapshots of DOPC-water system during the time that high fluctuations of the permeant position were recorded. The water molecule is represented by the van der Waals red sphere representing oxygen. The rest of the water molecules are transparent lines.

Permeability coefficients complete table

Table S4: Permeation coefficients and their logarithm of base 10, for a DOPC and a DOPC:DOPE(1:3) membrane, at T=300 K. PC refers to DOPC and PC:PE refers to DOPC:DOPE(1:3).

This work			Previous studies		
P $[\mathrm{cm\,s^{-1}}]$	logP	Membrane	P $[\mathrm{cm\,s^{-1}}]$	logP	Membrane
Urea					
$(6.74 \pm 3.03) \times 10^{-7}$	-6.17 ± 0.23	PC	5.37×10^{-7}	-6.27	$\mathrm{DMPC}_{298\,\mathrm{K}}$ [α, 14]
$(4.01 \pm 1.95) \times 10^{-7}$	-6.40 ± 0.25	PC:PE(1:3)	1.95×10^{-8}	-7.71	Model $\mathrm{SC}_{310\,\mathrm{K}}$ [α, 17]
			1.41×10^{-6}	-5.85	$\mathrm{DOPC}_{303\,\mathrm{K}}$ [β, 21]
			4.00×10^{-6}	-5.40	DMPC [β, 22]
			4.56×10^{-6}	-5.34	$\text{Caco-2}_{310\,\mathrm{K}}$ [β, 23]
Water					
$(3.96 \pm 0.39) \times 10^{-4}$	-3.40 ± 0.05	PC	6.80×10^{-2}	-1.17	$\mathrm{DMPC}_{320\,\mathrm{K}}$ [α, 24]
$(2.89 \pm 1.50) \times 10^{-4}$	-3.54 ± 0.27	PC:PE(1:3)	4.00×10^{-2}	-1.40	$\mathrm{DPPC}_{320\,\mathrm{K}}$ [α, 24]
			1.30×10^{-2}	-1.89	$\mathrm{DPPC}_{310\,\mathrm{K}}$ [δ, 25]
			1.60×10^{-2}	-1.80	$\mathrm{DPPC}_{323\,\mathrm{K}}$ [α, 26]
			7.00×10^{-2}	-1.15	$\mathrm{DPPC}_{350\,\mathrm{K}}$ [α, 27]
			1.40×10^{-3}	-2.85	DMPC $\mathrm{CG}_{303\,\mathrm{K}}$ [α, 18]
			1.58×10^{-2}	-1.80	$\mathrm{DOPC}_{303\,\mathrm{K}}$ [α, 28]
			1.30×10^{-2}	-1.89	$\mathrm{POPC}_{303\,\mathrm{K}}$ [α, 28]
			6.47×10^{-3}	-2.19	$\mathrm{POPC}_{308\,\mathrm{K}}$ [α, 29]
			8.30×10^{-3}	-2.08	$\mathrm{DMPC}_{303\,\mathrm{K}}$ [γ, 30]
			2.40×10^{-2}	-1.62	$\mathrm{DMPC}_{303\,\mathrm{K}}$ [β, 21]
			1.90×10^{-2}	-1.72	$\mathrm{DPPC}_{303\,\mathrm{K}}$ [β, 21]
			1.50×10^{-2}	-1.82	$\mathrm{DOPC}_{303\,\mathrm{K}}$ [β, 21]
			1.22×10^{-2}	-1.91	$\mathrm{DOPC}_{298\,\mathrm{K}}$ [β, 31]
			7.40×10^{-3}	-2.13	$\mathrm{DOPC{:}DOPE}_{298\,\mathrm{K}}$ [β, 31]
			4.26×10^{-3}	-2.37	$\mathrm{DOPC}_{294\,\mathrm{K}}$ [β, 32]
			5.20×10^{-4}	-3.28	$\mathrm{DMPC}_{343\,\mathrm{K}}$ [β, 33]
			2.30×10^{-6}	-5.64	$\mathrm{DMPE}_{343\,\mathrm{K}}$ [β, 33]
			3.00×10^{-4}	-3.52	$\mathrm{DPPC}_{343\,\mathrm{K}}$ [β, 33]
			3.70×10^{-6}	-5.43	$\mathrm{DPPE}_{343\,\mathrm{K}}$ [β, 33]
			6.00×10^{-4}	-3.22	DMPC_{fluid} [β, 34]
			2.30×10^{-4}	-3.64	$\mathrm{DOPC}_{293\,\mathrm{K}}$ [β, 34]
			1.50×10^{-2}	-1.82	$\mathrm{DLPC}_{298\,\mathrm{K}}$ [β, 35]
			3.40×10^{-3}	-2.47	$\mathrm{EPC}_{298\,\mathrm{K}}$ [β, 36]
			2.20×10^{-3}	-2.66	$\mathrm{EPC}_{298\,\mathrm{K}}$ [β, 37]
			1.90×10^{-3}	-2.72	$\mathrm{EPC}_{298\,\mathrm{K}}$ [β, 38]
			1.36×10^{-2}	-1.87	$\mathrm{POPC}_{298\,\mathrm{K}}$ [β, 39]
Glycine					
$(2.05 \pm 0.80) \times 10^{-3}$	-2.69 ± 0.20	PC	5.70×10^{-12}	-11.24	EPC [β, 40]
$(6.38 \pm 1.67) \times 10^{-4}$	-3.20 ± 0.14	PC:PE(1:3)	2.00×10^{-11}	-10.70	DMPC[β, 40]
			3.00×10^{-7}	-6.52	SC [β, 41]
Paracetamol					
$(3.76 \pm 1.17) \times 10^{-3}$	-2.42 ± 0.16	PC	7.30×10^{-6}	-5.14	$\mathrm{Permeapad}_{310\,\mathrm{K}}$ [β, 42]
$(9.44 \pm 5.10) \times 10^{-3}$	-2.03 ± 0.28	PC:PE(1:3)			
Ammonia					
$(6.58 \pm 1.57) \times 10^{-3}$	-2.18 ± 0.12	PC	1.30×10^{-1}	-0.89	$\mathrm{POPC}_{300\,\mathrm{K}}$ [α, 43]
$(1.91 \pm 0.26) \times 10^{-3}$	-2.72 ± 0.07	PC:PE(1:3)	1.70×10^{-2}	-1.77	$\mathrm{POPE}_{300\,\mathrm{K}}$ [α, 43]

Continued on next page

α: MD simulation, β: Experimental study, γ: Theoretical model, δ: Monte Carlo simulation

Table S4 – continued from previous page

This work			Previous studies		
P $\left[\mathrm{cm\,s^{-1}}\right]$	logP	Membrane	P $\left[\mathrm{cm\,s^{-1}}\right]$	logP	Membrane
			1.30×10^{-1}	-0.89	$\mathrm{DOPC}_{300\,\mathrm{K}}$ [α, 44]
			9.00×10^{-1}	-0.05	$\mathrm{DPPC}_{350\,\mathrm{K}}$ [α, 45]
			1.30×10^{-1}	-0.89	$\mathrm{EPC}_{298\,\mathrm{K}}$ [β, 36]
			4.80×10^{-2}	-1.32	DPhPC [β, 46]
			3.70×10^{-2}	-1.43	EPC [β, 47]
Ethanol					
$(1.55 \pm 0.24) \times 10^{-1}$	-0.81 ± 0.08	PC	8.50×10^{-2}	-1.07	$\mathrm{POPC}_{323\,\mathrm{K}}$ [α, 48]
$(1.08 \pm 0.32) \times 10^{-1}$	-0.97 ± 0.15	PC:PE(1:3)	1.12×10^{-5}	-4.95	Model $\mathrm{SC}_{310\,\mathrm{K}}$ [α, 17]
			2.00	0.30	$\mathrm{POPC}_{308\,\mathrm{K}}$ [α, 49]
			3.80×10^{-5}	-4.42	$\mathrm{SOPC}_{298\,\mathrm{K}}$ [β, 50]
			2.75×10^{-7}	-6.56	SC [γ, 51]
Isopropanol					
$(6.27 \pm 1.75) \times 10^{-1}$	-0.20 ± 0.15	PC			
$(3.34 \pm 0.68) \times 10^{-1}$	-0.48 ± 0.11	PC:PE(1:3)			
Coumarin					
1.14 ± 0.31	0.06 ± 0.14	PC	1.50×10^{-4}	-3.82	$\mathrm{Caco\text{-}2}_{310\,\mathrm{K}}$ [β, 52]
3.62 ± 0.48	0.56 ± 0.07	PC:PE(1:3)	7.76×10^{-5}	-4.11	$\mathrm{Caco\text{-}2}_{310\,\mathrm{K}}$ [β, 53]
			3.58×10^{-6}	-5.45	$\mathrm{Pig\ skin}_{310\,\mathrm{K}}$ [β, 54]
Fluoromethane					
3.86 ± 0.45	0.59 ± 0.06	PC			
4.07 ± 0.53	0.61 ± 0.07	PC:PE(1:3)			
Phenol					
5.03 ± 1.04	0.70 ± 0.11	PC	2.57	0.41	Model $\mathrm{SC}_{310\,\mathrm{K}}$ [α, 17]
2.40 ± 0.59	0.38 ± 0.13	PC:PE(1:3)	5.42×10^{-6}	-5.27	$\mathrm{SC}_{310\,\mathrm{K}}$ [β, 55]
Benzoic Acid					
6.27 ± 1.57	0.80 ± 0.13	PC	2.82	0.45	$\mathrm{DMPC}_{298\,\mathrm{K}}$ [α, 14]
8.19 ± 0.85	0.91 ± 0.05	PC:PE(1:3)	4.40×10^{-5}	-4.36	DOPC [β, 56]
			1.20×10^{-7}	-6.92	$\mathrm{DOPC}_{298\,\mathrm{K}}$ [β, 57]
			1.11×10^{-6}	-5.95	$\mathrm{DOPE}_{298\,\mathrm{K}}$ [β, 57]
			5.50×10^{-1}	-0.26	$\mathrm{EPC}_{298\,\mathrm{K}}$ [β, 36]
Propane					
7.33 ± 1.49	0.86 ± 0.11	PC			
7.28 ± 0.86	0.86 ± 0.06	PC:PE(1:3)			
Carbon dioxide					
10.00 ± 1.2	1.00 ± 0.06	PC	3.00	0.48	$\mathrm{POPC:POPE}_{300\,\mathrm{K}}$ [α, 43]
7.02 ± 0.56	0.85 ± 0.04	PC:PE(1:3)	3.20	0.51	$\mathrm{DPhPC}_{298\,\mathrm{K}}$ [β, 58]
			3.20×10^{-1}	-0.49	$\mathrm{EPC}_{296\,\mathrm{K}}$ [β, 59]

α: MD simulation, β: Experimental study, γ: Theoretical model, δ: Monte Carlo simulation

Hypothesis testing tables

Table S5: The logP values that were used for the hypothesis t-test

Permeant	logP		ΔlogP
	DOPC	DOPC:DOPE	
Ammonia	-2.18	-2.72	-0.54
Water	-3.40	-3.54	-0.14
Fluoromethane	0.59	0.61	0.02
Carbon dioxide	1.00	0.85	-0.16
Propane	0.86	0.86	0.00
Ethanol	-0.81	-0.97	-0.16
Urea	-6.17	-6.40	-0.23
Isopropanol	-0.20	-0.48	-0.27
Glycine	-2.69	-3.20	-0.51
Phenol	0.70	0.38	-0.32
Benzoic Acid	0.80	0.91	0.12
Coumarin	0.06	0.56	0.50
Paracetamol	-2.42	-2.03	0.40

Table S6: The analysis of the t-test.

	MW<100	MW>100	All
Mean:	-0.230	0.340	-0.098
Standard deviation:	0.188	0.201	0.309
Hypothesised mean (h):	0	0	0
t-statistic:	3.862	-2.933	1.144
Degrees of freedom:	9	2	12
Critical t-value (one-tailed):	1.833	2.920	1.782
Critical t-value (two-tailed) +-:	2.262	4.303	2.179
One-tailed probability P(h <x):	0.0019	0.950	0.137
One-tailed probability P(h >x):	0.998	0.0496	0.863
Two-tailed probability P(h = x):	0.004	0.099	0.275
Two-tailed probability P(h ≠ x):	0.996	0.901	0.725

Lateral mobility

Figures S8, S9 and S10 display the trajectories of the permeants over the 100 ns simulations with the DOPC bilayer, in relation to the simulation box (dashed lines). Similarly, figures S11, S12 and S13 present the permeant lateral mobility for the DOPC:DOPE bilayer. Different columns indicate different positions inside the bilayer and the rows are sorted based on the molecular weight of the permeants starting from the lightest.

Regarding the mobility between different depths, it is generally observed that the permeant diffuses faster in the water region (2.7 nm), then in the bilayer centre, then in the headgroup region (1.0 nm) and finally in the chain region (2.0 nm). These results are similar to the computed local diffusion profiles. Furthermore, the lateral mobility exhibits a "rattle-in-a-cage" behaviour where the permeant is trapped locally in pockets of free volume accompanied by fast transitions to neighbouring pockets, in agreement with previous reports.[19] Finally, there is no significant difference in the plots in terms of membrane composition. There seems to be a small increase in movement in the centre of the mixed bilayer which could be rationalised by the small increase in thickness which could leave some more free-space, although that could be compensated by the more ordered lipid chains.

In relation to the *lipid* lateral mobility, DOPC and DOPE in the liquid state (as in our work) are known to form ideal mixtures, with no evidence of clusters or other supermolecular structures (see Orsi and Essex[60] and relevant references therein). Furthermore, while previous studies have reported that certain additives (e.g, ethanol or other alcohols) may alter membrane dynamics, in order for their effect to be observable, higher concentrations than single molecules would be required. In our study, only a single permeant is present in each simulation box, so it is impossible to speculate whether this is enough to alter the physical properties of the membrane; we assume that none of the permeants did. We examined the systems visually to see whether the mixing properties of DOPC and DOPE changed when the permeant was inserted in the respective positions. However, during the 100 ns trajectories nothing unusual was observed for any of the positions.

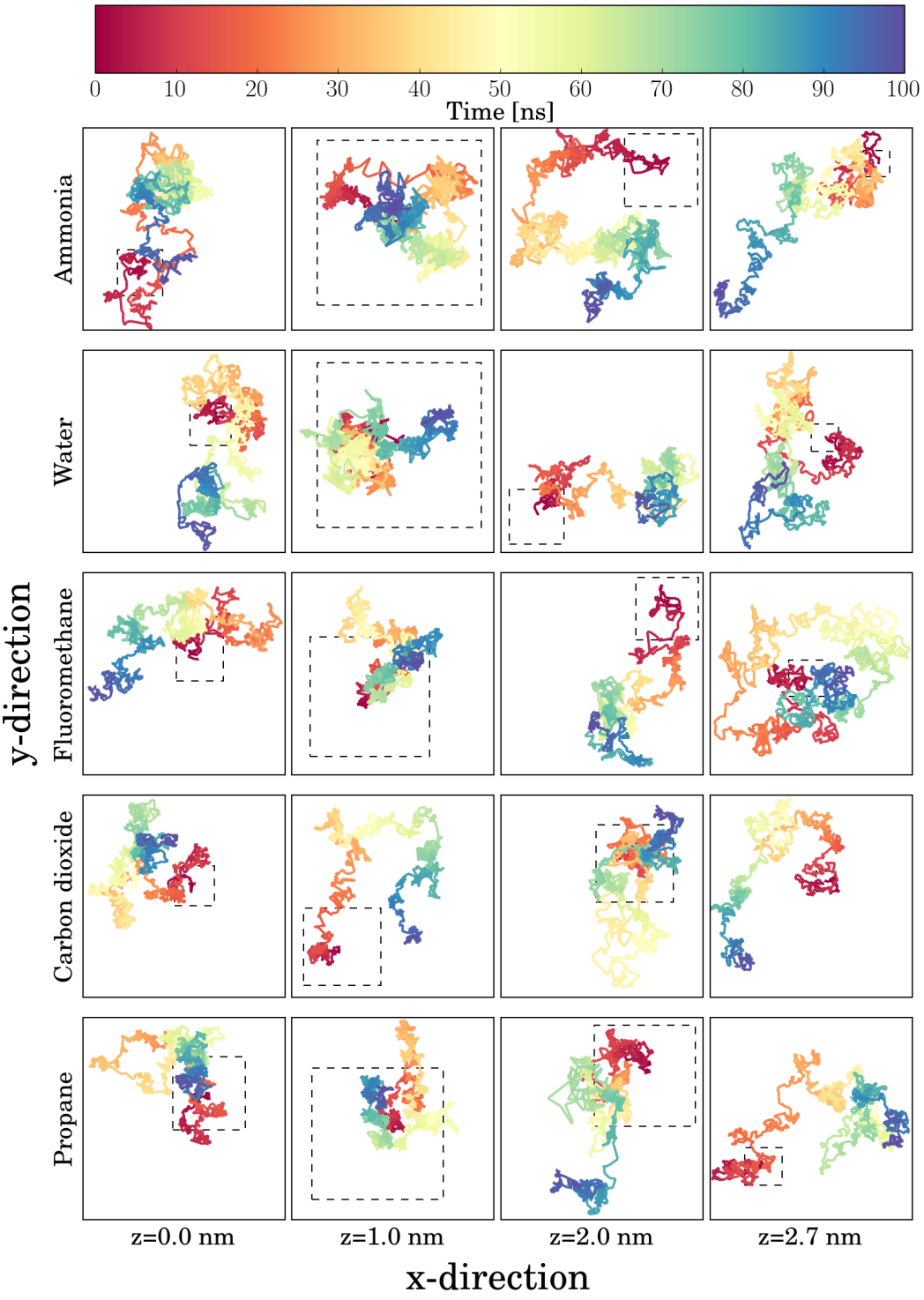

Figure S8: Lateral mobility of permeants in the DOPC membrane and in different depths; part A. Dashed lines indicate the simulation box (≈6 nm × 6 nm).

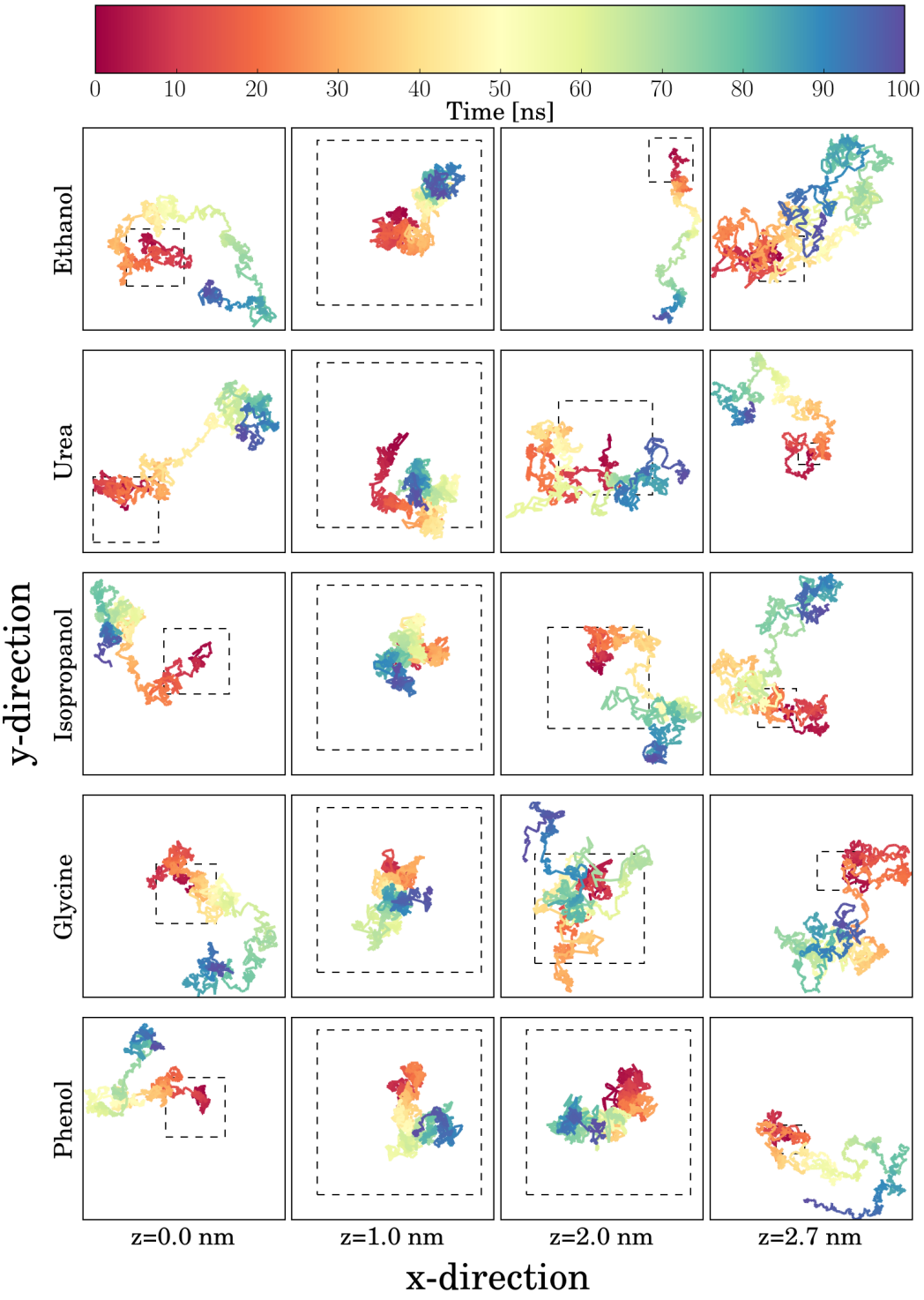

Figure S9: Lateral mobility of permeants in the DOPC membrane and in different depths; part B. Dashed lines indicate the simulation box (≈6 nm × 6 nm).

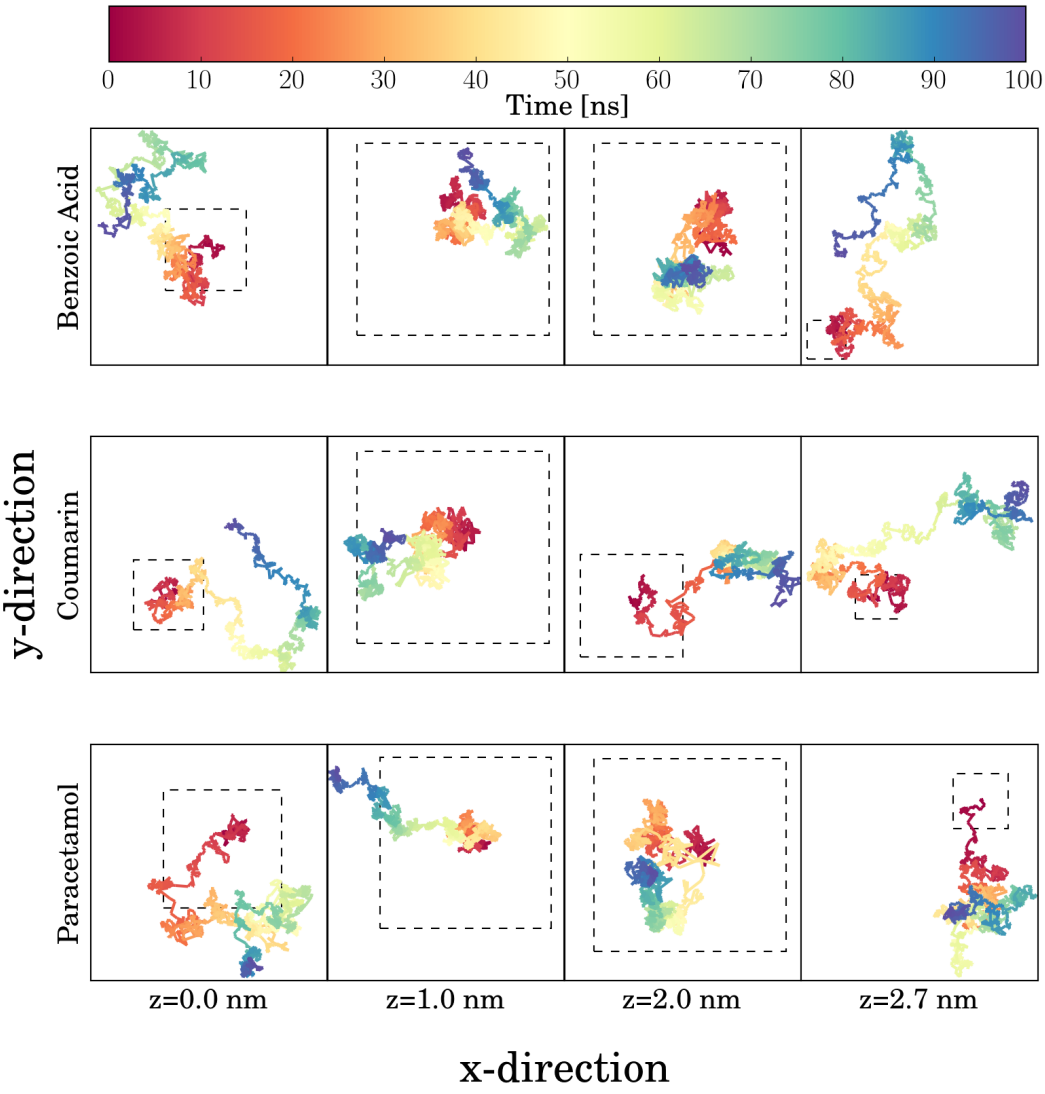

Figure S10: Lateral mobility of permeants in the DOPC membrane and in different depths; part C. Dashed lines indicate the simulation box (≈6 nm × 6 nm).

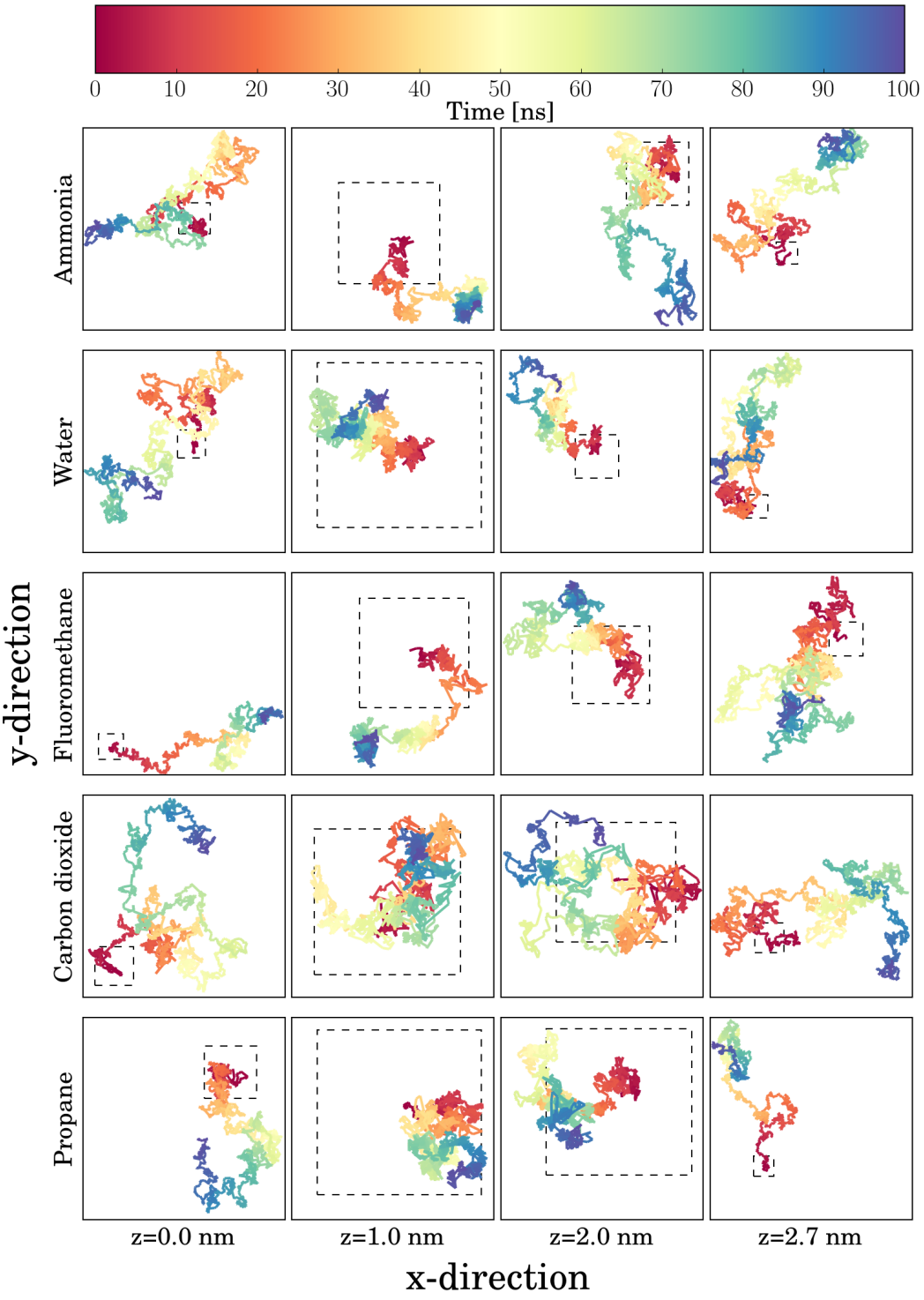

Figure S11: Lateral mobility of permeants in the DOPC:DOPE membrane and in different depths; part A. Dashed lines indicate the simulation box (≈6 nm × 6 nm).

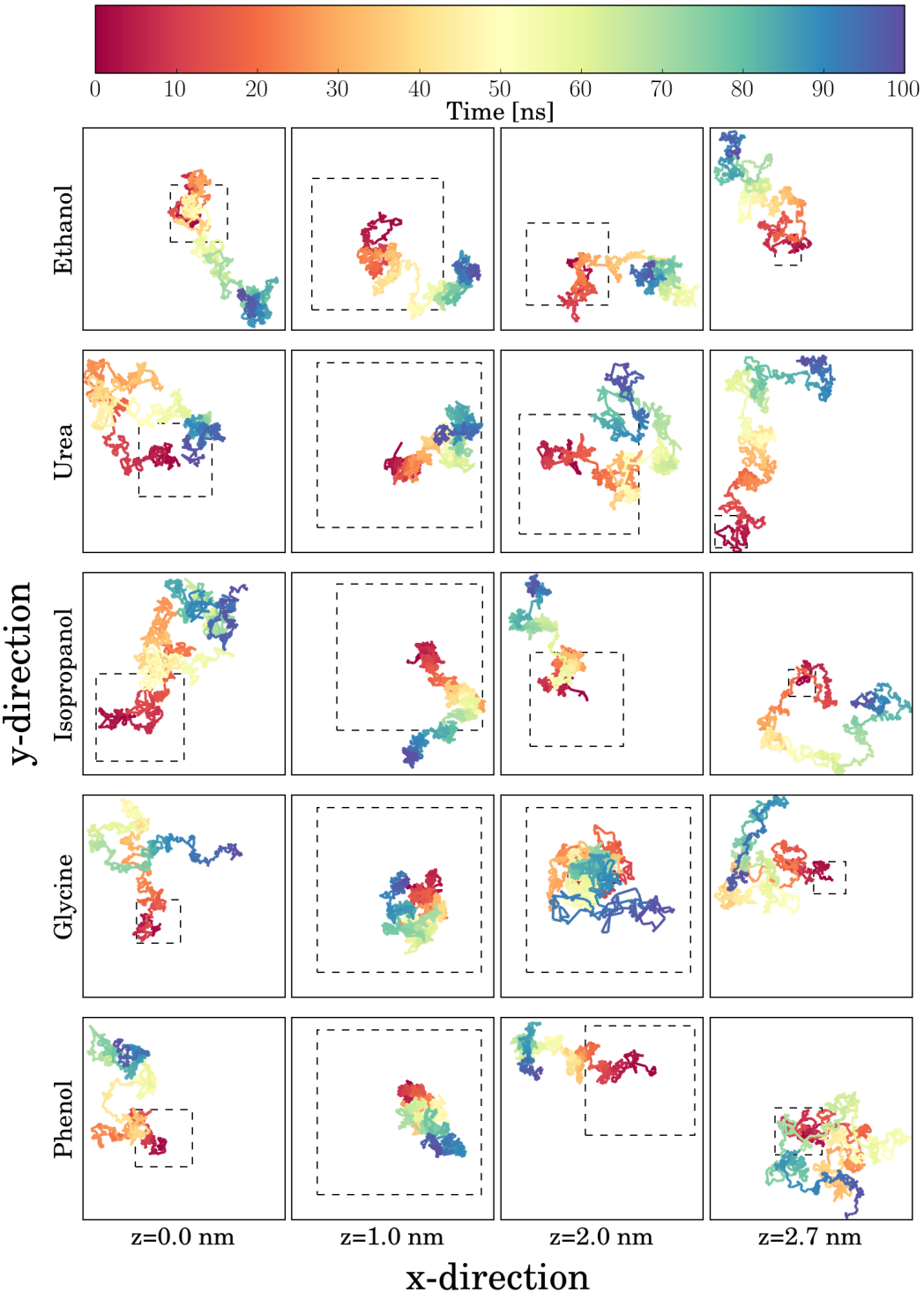

Figure S12: Lateral mobility of permeants in the DOPC:DOPE membrane and in different depths; part B. Dashed lines indicate the simulation box (≈6 nm × 6 nm).

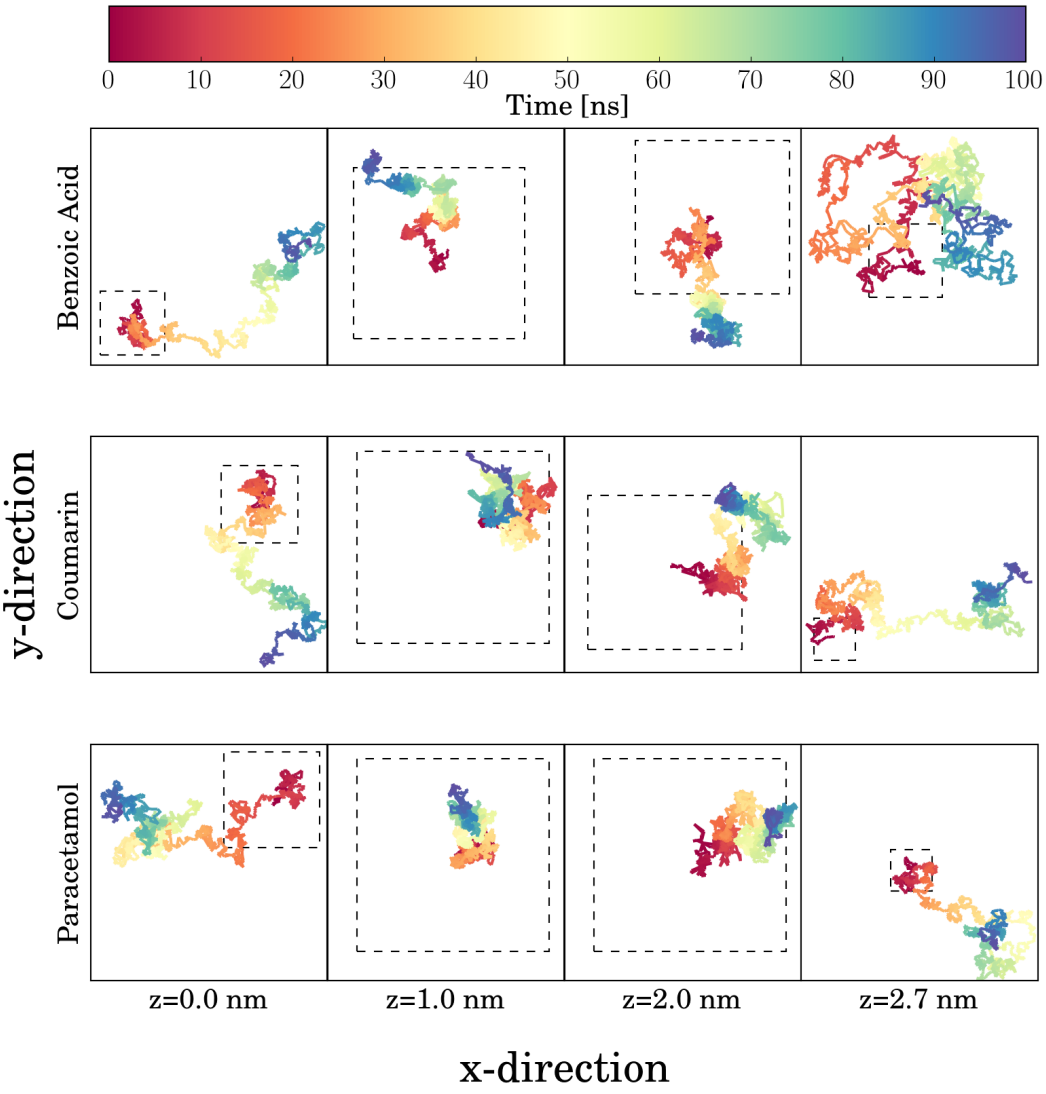

Figure S13: Lateral mobility of permeants in the DOPC:DOPE membrane and in different depths; part C. Dashed lines indicate the simulation box (≈6 nm × 6 nm).

References

(1) Viswanadhan, V. N.; Ghose, A. K.; Revankar, G. R.; Robins, R. K. Atomic physicochemical parameters for three dimensional structure directed quantitative structure-activity relationships. 4. Additional parameters for hydrophobic and dispersive interactions and their application for an automated superposition of certain naturally occurring nucleoside antibiotics. *J. Chem. Inf. Comput. Sci.* **1989**, *29*, 163–172.

(2) Sangster, J. Octanol Water Partition Coefficients of Simple Organic Compounds. *J. Phys. Chem. Ref. Data* **1989**, *18*, 1111–1229.

(3) Hansch, C. *Exploring QSAR*, 1st ed.; American Chemical Society, 1995.

(4) Grossfield, A.; Zuckerman, D. M. Chapter 2 Quantifying Uncertainty and Sampling Quality in Biomolecular Simulations. 2009; `http://dx.doi.org/10.1016/S1574-1400(09)00502-7`.

(5) Bemporad, D. Computer Simulation of Biological Membranes and Small Molecule Permeation. Ph.D. thesis, University of Southampton, 2003.

(6) Bemporad, D.; Luttmann, C.; Essex, J. W. Computer simulation of small moleculle permeation across a lipid bilayer: Dependence on bilayer properties and solute volume, size, and cross-sectional area. *Biophys. J.* **2004**, *87*, 1–13.

(7) Bemporad, D.; Essex, J. W.; Luttmann, C. Permeation of Small Molecules through a Lipid Bilayer: A Computer Simulation Study. *J. Phys. Chem. B* **2004**, *108*, 4875–4884.

(8) Bemporad, D.; Luttmann, C.; Essex, J. W. Behaviour of small solutes and large drugs in a lipid bilayer from computer simulations. *Biochim. Biophys. Acta* **2005**, *1718*, 1–21.

(9) Neale, C.; Bennett, W. F. D.; Tieleman, D. P.; Pomès, R. Statistical Convergence of Equilibrium Properties in Simulations of Molecular Solutes Embedded in Lipid Bilayers. *J. Chem. Theory Comput.* **2011**, *7*, 4175–4188.

(10) Flyvbjerg, H.; Petersen, H. G. G. Error estimates on averages of correlated data. *J. Chem. Phys.* **1989**, *91*, 461.

(11) Nitschke, N.; Atkovska, K.; Hub, J. S. Accelerating potential of mean force calculations for lipid membrane permeation: System size, reaction coordinate, solute-solute distance, and cutoffs. *J. Chem. Phys.* **2016**, *145*, 125101.

(12) Paloncýová, M.; Berka, K.; Otyepka, M. Convergence of free energy profile of coumarin in lipid bilayer. *J. Chem. Theory Comput.* **2012**, *8*, 1200–1211.

(13) Carpenter, T. S.; Kirshner, D. A.; Lau, E. Y.; Wong, S. E.; Nilmeier, J. P.; Lightstone, F. C. A Method to Predict Blood-Brain Barrier Permeability of Drug-Like Compounds Using Molecular Dynamics Simulations. *Biophys. J.* **2014**, *107*, 630–641.

(14) Lee, C. T.; Comer, J.; Herndon, C.; Leung, N.; Pavlova, A.; Swift, R. V.; Tung, C.; Rowley, C. N.; Amaro, R. E.; Chipot, C. et al. Simulation-Based Approaches for Determining Membrane Permeability of Small Compounds. *J. Chem. Inf. Model.* **2016**, *56*, 721–733.

(15) Hong, C.; Tieleman, D. P.; Wang, Y. Microsecond molecular dynamics simulations of lipid mixing. *Langmuir* **2014**, *30*, 11993–12001.

(16) O'neill, P. L.; Nicolaides, D.; Honnery, D.; Soria, J.; Others, Autocorrelation functions and the determination of integral length with reference to experimental and numerical data. 15th Australasian Fluid Mechanics Conference The University of Sydney, Sydney, Australia. 2004; pp 13–17.

(17) Gupta, R.; Sridhar, D. B.; Rai, B. Molecular Dynamics Simulation Study of Permeation of Molecules through Skin Lipid Bilayer. *J. Phys. Chem. B* **2016**, *120*, 8987–8996.

(18) Orsi, M.; Sanderson, W. E.; Essex, J. W. Permeability of small molecules through a lipid bilayer: a multiscale simulation study. *J. Phys. Chem. B* **2009**, *113*, 12019–12029.

(19) Orsi, M.; Essex, J. W. Permeability of drugs and hormones through a lipid bilayer: insights from dual-resolution molecular dynamics. *Soft Matter* **2010**, *6*, 3797.

(20) Carpenter, T. S.; Parkin, J.; Khalid, S. The Free Energy of Small Solute Permeation through the E. coli Outer Membrane has a Distinctly Asymmetric Profile. *J. Phys. Chem. Lett.* **2016**, *0*, null.

(21) Paula, S.; Volkov, A. G.; Van Hoek, A. N.; Haines, T. H.; Deamer, D. W. Permeation of protons, potassium ions, and small polar molecules through phospholipid bilayers as a function of membrane thickness. *Biophys. J.* **1996**, *70*, 339–348.

(22) Gallucci, E.; Micelli, S.; Lippe, C. Non-electrolyte permeability across thin lipid membranes. *Arch. Int. Physiol. Biochim.* **1971**, *79*, 881–887.

(23) Yazdanian, M.; Glynn, S. L.; Wright, J. L.; Hawi, A. Correlating partitioning and caco-2 cell permeability of structurally diverse small molecular weight compounds. *Pharm. Res.* **1998**, *15*, 1490–1494.

(24) Sugii, T.; Takagi, S.; Matsumoto, Y. A molecular-dynamics study of lipid bilayers: effects of the hydrocarbon chain length on permeability. *J. Chem. Phys.* **2005**, *123*, 184714.

(25) Jedlovszky, P.; Mezei, M. Calculation of the Free Energy Profile of H2O, O2, CO, CO2, NO, and CHCl3 in a Lipid Bilayer with a Cavity Insertion Variant of the Widom Method. *J. Am. Chem. Soc.* **2000**, *122*, 5125–5131.

(26) Shinoda, W.; Mikami, M.; Baba, T.; Hato, M. Molecular Dynamics Study on the Effects of Chain Branching on the Physical Properties of Lipid Bilayers: 2. Permeability. *J. Phys. Chem. B* **2004**, *108*, 9346–9356.

(27) Marrink, S.-J.; Berendsen, H. J. C. Simulation of water transport through a lipid membrane. *J. Phys. Chem.* **1994**, *98*, 4155–4168.

(28) Mathai, J. C.; Tristram-Nagle, S.; Nagle, J. F.; Zeidel, M. L. Structural determinants of water permeability through the lipid membrane. *J. Gen. Physiol.* **2008**, *131*, 69–76.

(29) Comer, J.; Schulten, K.; Chipot, C. Calculation of Lipid-Bilayer Permeabilities Using an Average Force. *J. Chem. Theory Comput.* **2014**, *10*, 554–564.

(30) Nagle, J. F.; Mathai, J. C.; Zeidel, M. L.; Tristram-Nagle, S. Theory of passive permeability through lipid bilayers. *J. Gen. Physiol.* **2008**, *131*, 77–85.

(31) Huster, D.; Jin, a. J.; Arnold, K.; Gawrisch, K. Water permeability of polyunsaturated lipid membranes measured by 17O NMR. *Biophys. J.* **1997**, *73*, 855–864.

(32) Olbrich, K.; Rawicz, W.; Needham, D.; Evans, E. Water permeability and mechanical strength of polyunsaturated lipid bilayers. *Biophys. J.* **2000**, *79*, 321–327.

(33) Jansen, M.; Blume, A. A comparative study of diffusive and osmotic water permeation across bilayers composed of phospholipids with different head groups and fatty acyl chains. *Biophys. J.* **1995**, *68*, 997–1008.

(34) Carruthers, A.; Melchior, D. L. Studies of the Relationship between Bilayer Water Permeability and Bilayer Physical State? *Biochemistry* **1983**, *22*, 5797–5807.

(35) Lande, M. B.; Donovan, J. M.; Zeidel, M. L. The relationship between membrane fluidity and permeabilities to water, solutes, ammonia, and protons. *J. Gen. Physiol.* **1995**, *106*, 67–84.

(36) Walter, A.; Gutknecht, J. Permeability of small nonelectrolytes through lipid bilayer membranes. *J. Membr. Biol.* **1986**, *90*, 207–217.

(37) Finkelstein, A. Water and nonelectrolyte permeability of lipid bilayer membranes. *J. Gen. Physiol.* **1976**, *68*, 127–135.

(38) Xiang, T. X.; Anderson, B. D. The relationship between permeant size and permeability in lipid bilayer membranes. *J. Membr. Biol.* **1994**, *140*, 111–122.

(39) Koenig, S. H.; Ahkong, Q. F.; Brown, R. D., 3rd; Lafleur, M.; Spiller, M.; Unger, E.; Tilcock, C. Permeability of liposomal membranes to water: results from the magnetic field dependence of T1 of solvent protons in suspensions of vesicles with entrapped paramagnetic ions. *Magn. Reson. Med.* **1992**, *23*, 275–286.

(40) Chakrabarti, A. C.; Deamer, D. W. Permeability of lipid bilayers to amino acids and phosphate. *Biochim. Biophys. Acta* **1992**, *1111*, 171–177.

(41) Arct, J.; Chelkowska, M.; Kasiura, K.; Pietrzykowski, P. The fatty acids as penetration enhancers of amino acids by ion pairing. *Int.J.Cosmet.Sci.* **2002**, *24*, 313–322.

(42) di Cagno, M.; Bibi, H. A.; Bauer-Brandl, A. New biomimetic barrier Permeapad$^{\mathrm{TM}}$ for efficient investigation of passive permeability of drugs. *Eur. J. Pharm. Sci.* **2015**, *73*, 29–34.

(43) Hub, J. S.; Winkler, F. K.; Merrick, M.; De Groot, B. L. Potentials of mean force and permeabilities for carbon dioxide, ammonia, and water flux across a Rhesus protein channel and lipid membranes. *J. Am. Chem. Soc.* **2010**, *132*, 13251–13263.

(44) Zocher, F.; Van Der Spoel, D.; Pohl, P.; Hub, J. S. Local partition coefficients govern solute permeability of cholesterol-containing membranes. *Biophys. J.* **2013**, *105*, 2760–2770.

(45) Marrink, S. J.; Berendsen, H. J. C. Permeation process of small molecules across lipid membranes studied by molecular dynamics simulations. *J. Phys. Chem.* **1996**, *100*, 16729–16738.

(46) Antonenko, Y. N.; Pohl, P.; Denisov, G. A. Permeation of ammonia across bilayer lipid membranes studied by ammonium ion selective microelectrodes. *Biophys. J.* **1997**, *72*, 2187–2195.

(47) Antonenko, Y. N.; Yaguzhinsky, L. S. The role of pH gradient in the unstirred layers in the transport of weak acids and bases through bilayer lipid membranes. *Bioelectrochem. Bioenerg.* **1984**, *13*, 85–91.

(48) Ghaemi, Z.; Minozzi, M.; Carloni, P.; Laio, A. A novel approach to the investigation of passive molecular permeation through lipid bilayers from atomistic simulations. *J. Phys. Chem. B* **2012**, *116*, 8714–8721.

(49) Comer, J.; Schulten, K.; Chipot, C. Diffusive Models of Membrane Permeation with Explicit Orientational Freedom. *J. Chem. Theory Comput.* **2014**, *10*, 2710–2718.

(50) Ly, H. V.; Longo, M. L. The influence of short-chain alcohols on interfacial tension, mechanical properties, area/molecule, and permeability of fluid lipid bilayers. *Biophys. J.* **2004**, *87*, 1013–1033.

(51) Abraham, M. H.; Martins, F.; Mitchell, R. C. Algorithms for Skin Permeability Using Hydrogen Bond Descriptors: the Problem of Steroids*. *J. Pharm. Pharmacol.* **1997**, *49*, 858–865.

(52) Galkin, A.; Fallarero, A.; Vuorela, P. M. Coumarins permeability in Caco-2 cell model. *J. Pharm. Pharmacol.* **2009**, *61*, 177–184.

(53) Camenisch, G.; Alsenz, J.; van de Waterbeemd, H.; Folkers, G. Estimation of permeability by passive diffusion through Caco-2 cell monolayers using the drugs' lipophilicity and molecular weight. *Eur. J. Pharm. Sci.* **1998**, *6*, 317–324.

(54) Pan, T.-L.; Wang, P.-W.; Aljuffali, I. A.; Leu, Y.-L.; Hung, Y.-Y.; Fang, J.-Y. Coumarin derivatives, but not coumarin itself, cause skin irritation via topical delivery. *Toxicol. Lett.* **2014**, *226*, 173–181.

(55) Singh, P.; Roberts, M. S. Skin permeability and local tissue concentrations of nons-

teroidal anti-inflammatory drugs after topical application. *J. Pharmacol. Exp. Ther.* **1994**, *268*, 144–151.

(56) Ruell, J. A.; Tsinman, K. L.; Avdeef, A. PAMPA–a drug absorption in vitro model. 5. Unstirred water layer in iso-pH mapping assays and pKa(flux)–optimized design (pOD-PAMPA). *Eur. J. Pharm. Sci.* **2003**, *20*, 393–402.

(57) Seo, P. R.; Teksin, Z. S.; Kao, J. P. Y.; Polli, J. E. Lipid composition effect on permeability across PAMPA. *Eur. J. Pharm. Sci.* **2006**, *29*, 259–268.

(58) Missner, A.; Kügler, P.; Saparov, S. M.; Sommer, K.; Mathai, J. C.; Zeidel, M. L.; Pohl, P. Carbon dioxide transport through membranes. *J. Biol. Chem.* **2008**, *283*, 25340–25347.

(59) Gutknecht, J.; Bisson, M. A.; Tosteson, F. C. Diffusion of carbon dioxide through lipid bilayer membranes: effects of carbonic anhydrase, bicarbonate, and unstirred layers. *J. Gen. Physiol.* **1977**, *69*, 779–794.

(60) Orsi, M.; Essex, J. W. Physical properties of mixed bilayers containing lamellar and nonlamellar lipids: insights from coarse-grain molecular dynamics simulations. *Faraday Discuss.* **2013**, *161*, 249–272.